AMERICAN SOCIETY FOR MICROBIOLOGY | Journal of Virology

Five of Five VHHs Neutralizing Poliovirus Bind the Receptor-Binding Site

Mike Strauss,[a] Lise Schotte,[b,c] Bert Thys,[b] David J. Filman,[a] James M. Hogle[a]

Department of Biological Chemistry and Molecular Pharmacology, Harvard Medical School, Boston, Massachusetts, USA[a]; Department of Pharmaceutical Biotechnology and Molecular Biology, Center for Neurosciences, Vrije Universiteit Brussel, Brussels, Belgium[b]; Department of Clinical Chemistry and Radio-immunology, Universitair Ziekenhuis Brussel, Brussels, Belgium[c]

ABSTRACT

Nanobodies, or VHHs, that recognize poliovirus type 1 have previously been selected and characterized as candidates for antiviral agents or reagents for standardization of vaccine quality control. In this study, we present high-resolution cryo-electron microscopy reconstructions of poliovirus with five neutralizing VHHs. All VHHs bind the capsid in the canyon at sites that extensively overlap the poliovirus receptor-binding site. In contrast, the interaction involves a unique (and surprisingly extensive) surface for each of the five VHHs. Five regions of the capsid were found to participate in binding with all five VHHs. Four of these five regions are known to alter during the expansion of the capsid associated with viral entry. Interestingly, binding of one of the VHHs, PVSS21E, resulted in significant changes of the capsid structure and thus seems to trap the virus in an early stage of expansion.

IMPORTANCE

We describe the cryo-electron microscopy structures of complexes of five neutralizing VHHs with the Mahoney strain of type 1 poliovirus at resolutions ranging from 3.8 to 6.3Å. All five VHHs bind deep in the virus canyon at similar sites that overlap extensively with the binding site for the receptor (CD155). The binding surfaces on the VHHs are surprisingly extensive, but despite the use of similar binding surfaces on the virus, the binding surface on the VHHs is unique for each VHH. In four of the five complexes, the virus remains essentially unchanged, but for the fifth there are significant changes reminiscent of but smaller in magnitude than the changes associated with cell entry, suggesting that this VHH traps the virus in a previously undescribed early intermediate state. The neutralizing mechanisms of the VHHs and their potential use as quality control agents for the end game of poliovirus eradication are discussed.

In addition to conventional antibodies, members of the Camelidae family possess a set of unusual antibodies that consist only of heavy chains in which a constant domain is missing and that are therefore named heavy-chain-only antibodies (1). These antibodies offer a very interesting new tool in scientific research, as they contain variable domains (VHHs) that are fully responsible for and fully capable of recognizing and binding to antigens. The variable domains are also more hydrophilic than their IgG counterparts, as they are not required to bind to a complementary domain of a light chain. Moreover, they are very stable (2), and due to their rather small size (~14 kDa), they are able to bind to epitopes within clefts (3) that are more difficult to reach for larger antibodies. Both their single-domain nature and their lack of glycosylation allow them to be produced at high levels using bacterial expression systems.

Motivated by searches for potential antiviral agents, VHHs that specifically bind to and neutralize poliovirus type 1 were recently selected and identified (4) and were further characterized (5, 6). In a previous publication (5), we showed that the binding footprints of two VHHs (PVSP6A and PVSP29F) on the poliovirus surface overlap extensively with the footprint of the poliovirus receptor (PVR; also called CD155) and that they produce well-ordered icosahedrally symmetric complexes. It was also shown that the mechanisms of neutralization operate at multiple stages of the infection process and that all of the neutralizing VHHs stabilize the virus to prevent viral expansion (5), which is an essential step in the infection of cells.

As a member of the *Picornaviridae* family, poliovirus is a naked virus comprised only of a protein capsid surrounding its positively single-stranded RNA. The capsid has a pseudo T=3 icosahedral surface with 60 copies of each of four viral proteins (VPs), VP1 to VP4, of which VP4, the smallest one, is myristoylated at its N terminus (7) and is found on the inner surface of the capsid. VP1 to VP3 each include a large wedge-shaped eight-stranded beta barrel (which are packed together, side by side, to form the outer surface of the capsid) and have long, flexible loops and terminal extensions that bind to the upper and lower surfaces of neighboring beta barrels (thus contributing their binding energies to stabilization). As a metastable structure, the capsid protects the genome in most environments. However, when the virus interacts with PVR at physiological temperature, the receptor catalyzes a

Received 29 November 2015 **Accepted** 8 January 2016

Accepted manuscript posted online 13 January 2016

Citation Strauss M, Schotte L, Thys B, Filman DJ, Hogle JM. 2016. Five of five VHHs neutralizing poliovirus bind the receptor-binding site. J Virol 90:3496–3505. doi:10.1128/JVI.03017-15.

Editor: T. S. Dermody

Address correspondence to James M. Hogle, james_hogle@hms.harvard.edu.

M.S. and L.S. are co-first authors.

Supplemental material for this article may be found at http://dx.doi.org/10.1128/JVI.03017-15.

program of conformation alterations (8) that lead to the expansion of the virion (which sediments at 160S) and to the externalization of two polypeptides (the myristoylated protein VP4 [9] and the N terminus of VP1 [10]) to form an intermediate that sediments at 135S (the 135S particle) (9, 11). The externalized peptides are inserted into the plasma membrane (12) and the particle is internalized into endosomes (13). The inserted peptides then facilitate the translocation of the viral genome across the endosomal membrane and into the cytoplasm to initiate infection, leaving an empty particle which sediments at 80S (the 80S particle).

The native virion (the 160S particle) defines the D- or N-antigenic state of the virus (14). The 135S and 80S particles share antigenicity with heat-inactivated virus (9, 11), which defines the C- or H-antigenic state of the virus (14). The D antigen, but not the C antigen, elicits neutralizing antibodies (15).

The receptor is known to interact with the capsid in the canyon (16, 17), a depression surrounding the star-shaped plateau at the 5-fold axis of symmetry. At the base of the canyon, the beta barrel of VP1 includes a hydrophobic pocket that is the binding site for a hydrophobic compound, called the pocket factor (18). In the poliovirus structures solved to date, the pocket factor has been modeled as one of several fatty acid-like molecules, including sphingosine and palmitate. Using cryo-electron microscopy (cryo-EM) reconstructions of the complex between poliovirus and the three ectodomains of CD155 at subphysiological temperature, it has recently been shown that nectin-like interactions of the virus with the receptor result in the expulsion of the pocket factor and subtle changes in the structure of the virion that prime the particle for expansion when the temperature is raised (19).

Here we report cryo-EM reconstructions, at a nearly atomic resolution, of the complexes between poliovirus type 1 and each of five neutralizing D-specific VHHs. By noting what portions of the binding footprints that the complexes have in common and identifying the specific intermolecular interactions in the complexes, we try to explain the mechanism of stabilization and neutralization in nearly atomic detail.

MATERIALS AND METHODS

Virus. The poliovirus type 1 Mahoney strain was grown in HeLa cells in suspension. After infection with Mahoney (multiplicity of infection = 10) and incubation at 37°C for 6 h, the cells were collected by centrifugation. The pellet was freeze-thawed three times, and the cell debris was removed. Virus was pelleted by ultracentrifugation and purified over a CsCl density gradient. Finally, the collected virus fraction was dialyzed against phosphate-buffered saline (PBS; 137 mM NaCl, 2.7 mM KCl, 1.1 mM KH_2PO_4, 6.5 mM Na_2HPO_4, 0.7 mM $CaCl_2$, 0.5 mM $MgCl_2$) and stored at −80°C. The Mahoney strain used in this study differs from the reference Mahoney strain (NCBI GenBank accession number V01149.1), in that it contains two substitutions in the capsid proteins: F123S in VP3 and L228I in VP1.

VHHs. The selection, production, and purification of the VHHs were previously described in detail (4, 5). Originally, the VHHs used in these experiments were obtained from a dromedary immunized against poliovirus type 1. Peripheral blood lymphocytes were collected 6 weeks after the immunization, and RNA was extracted and reverse transcribed. The VHH-encoding cDNA was cloned into the phagemid vector pHEN4 (2) for phage display panning on immobilized poliovirus type 1 and recloned into vector pHEN6(c) for expression in *Escherichia coli* WK6 cells. Finally, the VHHs were purified as described previously (5) and stored at −80°C in Tris buffer (137 mM NaCl, 25 mM Tris, pH 7.2). Five different recombinant VHHs were used: PVSP6A, PVSS8A, PVSP19B, PVSS21E, and PVSP29F. They all show an *in vitro* neutralizing activity against poliovirus type 1 at nanomolar concentrations (4).

Cryo-electron microscopy. Samples for cryo-electron microscopy were prepared as described by Schotte et al. (5). Briefly, 4 μl of VHH (1 mg/ml in Tris buffer) was added to 10 μl of poliovirus (0.9 mg/ml) in PBS buffer at 4°C, resulting in a ±300-fold molar excess of VHH. A 3-μl droplet of the resulting solution/mixture was added to the surface of a glow-discharged perforated carbon support (C-flat 1.2/1.3; Protochips), and the excess was removed by blotting with filter paper (Whatman no. 1) before the carbon support was plunged into liquid ethane slush. The imaging and reconstruction of PVSP6A and PVSP29F have been reported in Schotte et al. (5). The grids of the other VHHs were imaged in a Polara G2 electron microscope (FEI Co.) at 300 kV using a K2 Summit direct detector (Gatan Inc.) in superresolution mode, such that the final pixel size was 0.985 Å. Over a span of 12 s, 24 frames were recorded for each acquisition, using a dose rate of 8 electrons/pixel/s. The frames in the individual movies were aligned and summed using the dosef program (20), with the first two frames, which showed the most drift, being discarded. The estimation of the contrast transfer function was carried out on the summed images with the ctffind3 program (21), and particles were picked using a semiautomated algorithm in the e2boxer.py program (22). The boxed particles were then subjected to two- and three-dimensional classification in the Relion1.2 program (23), using poliovirus Fourier filtered to a 40-Å resolution as a reference, and the most consistent classes were kept for the final refinement. The three-dimensional class average was used as a reference for the final iterative refinement procedure, which was done using the GeFrealign program (24). The Fourier terms used for refinement were limited to the resolution regimes that had higher correlation statistics between half-set reconstructions, typically better than 0.7 in the Fourier shell correlation (FSC) plot. This procedure avoids the introduction of model bias (25). The final maps were sharpened by applying a negative B factor in the most recent version of the Frealign (v9.09) program (26).

Construction of the models. Atomic models were constructed and refined to fit each of the maps (using the COOT, SPDBV, and Refmac5 programs; see the refinement statistics in Table 1), using the Fourier transform of a portion of the reconstruction (both amplitudes and phases) as refinement standards, with symmetry-related neighboring proteins being present, with icosahedral symmetry being strongly enforced, and with idealized stereochemical standards being applied as restraints. Portions of each model where the density exhibited significant differences from the structural homologs (identified using the vector alignment search tool [http://structure.ncbi.nlm.nih.gov/Structure/VAST/vastsearch.html]) were subjected to an all-atom refinement, while the core regions that were in good agreement with the homologous model were restrained to resemble a rigid-body docking. The resolution limits and statistics of the atomic model refinement of each of the complexes are shown in Table 1.

Protein structure accession numbers. The refined atomic coordinates and cryo-EM reconstructions of the complexes of poliovirus type 1 with each of the five VHHs can be found in the Protein Data Bank (PDB) and the Electron Microscopy Data Bank (EMBD): for PVSP6A, PDB accession number 3JBD and EMDB accession number 5886; for PVSP29F, PDB accession number 3JBC and EMDB accession number 5888; for PVSS8A, PDB accession number 3JBE and EMDB accession number 6433; for PVSP19B, PDB accession number 3JBF and EMDB accession number 6434; and for PVSS21E, PDB accession number 3JBG and EMDB accession number 6435.

RESULTS

Cryo-EM reconstructions of five VHH-poliovirus complexes were calculated, and the resulting maps were analyzed to produce pseudoatomic models describing the structures. All five VHHs were found to bind at or near the quasi-3-fold axis of the virus (Fig. 1).

Resolution. The structures of the VHH-poliovirus complexes

TABLE 1 Statistics for reconstructions and refinement of atomic models

	Value for the following complex:				
VHH	PVSP6A	PVSS8A	PVSP19B	PVSS21E	PVSP29F
Resolution (Å)[a]	98–4.7	95–4.2	95–4.6	96–3.8	98–5.6
No. of pseudoreflections	205,969	272,424	207,238	377,722	129,932
wFOM[c]	0.542	0.626	0.508	0.530	0.506
R_{factor} (%)	43.3	41.2	46.5	42.8	42.8
R_{factor} for outer shell (%)	47.3	51.7	54.1	53.0	54.4
FOM[c] (Refmac5)	0.794	0.788	0.773	0.747	0.826
Bond error (Å)	0.008	0.012	0.010	0.008	0.010
Angle error (°)	1.771	2.346	2.10	1.753	2.320
Resolution (FSC, 0.143)[b]	4.9	4.2	4.8	3.8	6.3
Grid spacing (Å)	1.681	0.985	0.985	0.985	1.681
Sampling grid	320 × 320 × 320	512 × 512 × 512	512 × 512 × 512	512 × 512 × 512	320 × 320 × 320
Submap size	128 × 140 × 120	216 × 216 × 216	216 × 216 × 216	216 × 216 × 216	128 × 140 × 128
Submap origin	−56,−49,0	−80,−64,0	−80,−64,0	−80,−64,0	−56,−49,0
Microscope	FEI Titan Krios	FEI Polara G2	FEI Polara G2	FEI Polara G2	FEI Titan Krios
Voltage (kV)	200	300	300	300	200
Emitter	Field emission gun	Field emission gun	Field emission gun	Field emission gun	Field emission gun
Detector	Gatan US 4000	Gatan K2 Summit	Gatan K2 Summit	Gatan K2 Summit	Gatan US 4000
No. of particles	57,282	16,421	18,009	24,717	9,764
No. of VHH amino acids	1–120	1–127	1–123	1–121	1–129
PDB accession no.					
Structural homolog	4BEL	4I0C	1I3U	3QXU	1QD0
Poliovirus-VHH complex	3JBD	3JBE	3JBF	3JBG	3JBC
EMDB accession no.	5886	6433	6434	6435	5888

[a] The resolution range used in the refinement. The high-resolution limit is based on where the amplitudes and phases calculated on the basis of the model correlate with those calculated on the basis of the Fourier transform of the map.
[b] The resolution where the Fourier shell correlation falls below 0.143. For high-resolution structures, this is generally a conservative estimate of the resolution and may be of a lower resolution than the apparent resolution based on comparisons of the transforms of the model and map.
[c] Figures of merit compare Fourier phases from the experimental map with phases from the atomic model (with 1.0 indicating perfect phase agreement, and 0.0 indicating a complete lack of correlation). wFOM is the Fourier-amplitude-weighted average of the cosine of the phase discrepancy. FOM is the unweighted average.

solved by cryo-EM are of sufficient resolution to unambiguously identify the orientation of binding for all five VHHs examined. Portions of each model where the density exhibited significant differences from that of the structural homologs were subjected to an all-atom refinement, while the core regions that were in good agreement with the homologous model were restrained to resemble a rigid-body docking. The nominal resolutions of the reconstructions are as follows: PVSP6A, 4.9 Å; PVSS8A, 4.2 Å; PVSP19B, 4.8 Å; PVSS21E, 3.8 Å; and PVSP29F, 6.3 Å (see the FSC curves in Fig. 1 and statistics for the reconstructions in Table 1).

For poliovirus, the resulting models include VP1 (residues 20 to 302), VP2 (residues 8 to 272), VP3 (residues 1 to 235), VP4 (residues 1 to 69 and the N-terminal myristate), and palmitate noncovalently bound in the center of the VP1 beta barrel. Each VHH has about 125 ordered amino acids (as specified in Fig. 2), including some number of partially ordered histidines from the His_6 tag at its carboxyl terminus.

Quality of model fit to density. Qualitatively, the fit of the refined atomic models to the density in the reconstructions is excellent (Fig. 3). In general, the quality and strength of the map features vary by radius, with the lower-radius portions of the poliovirus beta barrels being the strongest and best defined and the highest-radius (carboxyl-end) portions of the bound VHHs being weaker and less well defined. This radial discrepancy is likely due to the greater impact of orientation errors at a high radius, though structural heterogeneity in the complexes may contribute as well.

With the exception of PVSP29F, the beta strands in poliovirus and in most of the VHHs are well resolved with an appropriate choice of contour level, though there is rarely a single choice of contour level that works consistently well throughout the map. In general, the correspondence between the density and the main chain trace is unambiguous, the docked model is clearly similar in shape to the density, and the densities for most of the loops and terminal extensions are clear. In the best resolved of the maps (Fig. 3), many of the side chains are obvious as well, with the density map (and/or chemical considerations) providing indications for the correct choice of side chain rotamer.

As an important aspect of the modeling and refinement procedure, we also identified a core portion of each VHH domain and each poliovirus capsid protein that refines to resemble part of a known crystal structure (see Materials and Methods). In Table 2, we identify structural homologs for each VHH and the residues that were included in its rigid-body core. In four of the complexes, the structure of poliovirus proteins strongly resembles the 2.2-Å-resolution model of mature poliovirions obtained with the structure with PDB accession number 1HXS (with only minor localized changes due to direct VHH binding being seen). The exception was capsid protein VP1 in its complex with VHH PVSS 21E, which showed extensive regions of difference (Fig. 4). In the Discussion, we specify the regions of greatest difference and discuss the possibility that binding to VHH PVSS21E may have

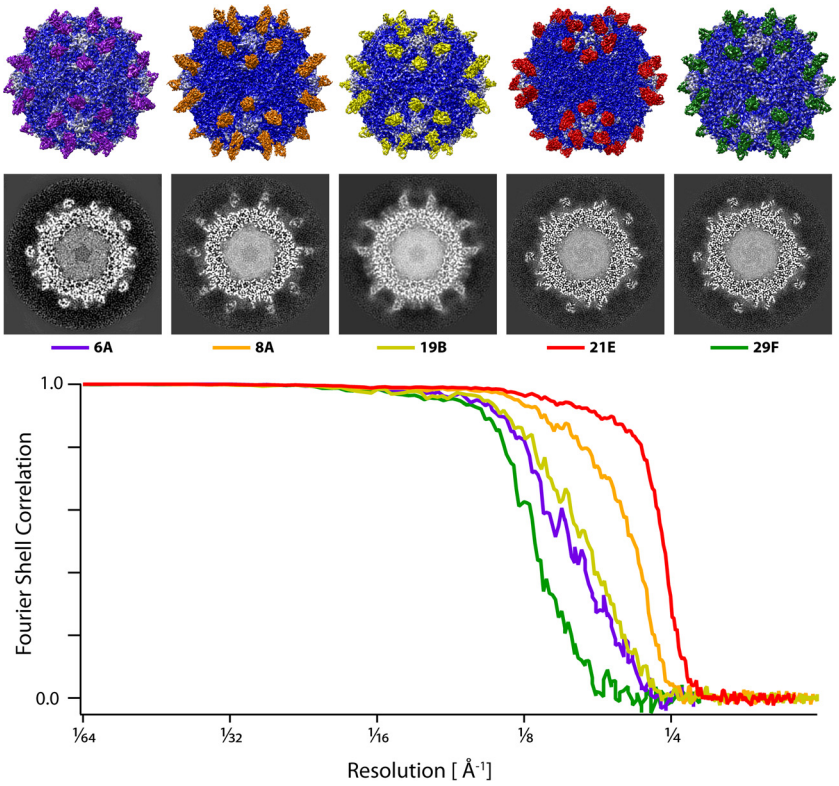

FIG 1 Cryo-EM reconstructions of five poliovirus-VHH complexes. (Top) From left to right, the complexes of poliovirus (blue) with PVSP6A (6A; purple), PVSS8A (8A; orange), PVSP19B (19B; yellow), PVSS21E (21E; red), and PVSP29F (29F; green) are shown as isocontour surfaces that are shaded by radius and depth. (Middle) Representative density slices are shown for each of the complexes. Each slice is viewed along a 5-fold axis. Note that each VHH binds to the capsid in a slightly different spot. (Bottom) Fourier shell correlation (FSC) curves are plotted for the complexes of poliovirus type 1 with PVSP6A (purple), PVSS8A (orange), PVSP19B (yellow), PVSS21E (red), and PVSP29F (green). The upper-resolution limits for the 0.143 criterion range from 3.8 to 6.3 Å. (Reconstructions for PVSP6A and PVSP29F are republished from reference 5.)

trapped the virus in a native-like alternative conformation that normally occurs during the early stages of reversible expansion.

Statistics of fit. For each of the five poliovirus-VHH complexes, the quality of the overall fit can be put on a quantitative basis by comparing the Fourier transform of the model-based electron density to the Fourier transform of the corresponding portion of the cryo-EM map (agreement statistics are listed in Table 1). Thus, Refmac5 (27) reports the Fourier amplitude agreement with an R factor and Fourier phase agreement with a figure of merit. Externally, using the SFTOOLS program (B. Hazes, unpublished data), we also tracked the Fourier-amplitude-weighted average of the cosine of the phase discrepancy, which is analogous to a crystallographic figure of merit (with 1.0 indicating perfect phase agreement and 0.0 indicating a complete lack of correla-

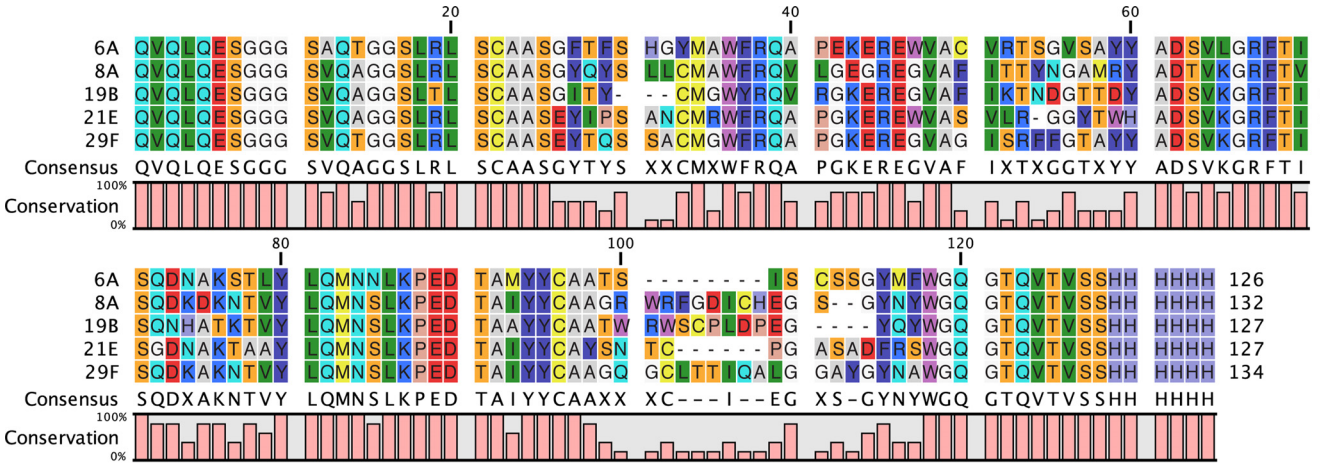

FIG 2 VHH amino acid sequence alignment. The amino acid sequences of the five VHHs are shown and were aligned using the CLC Sequence viewer.

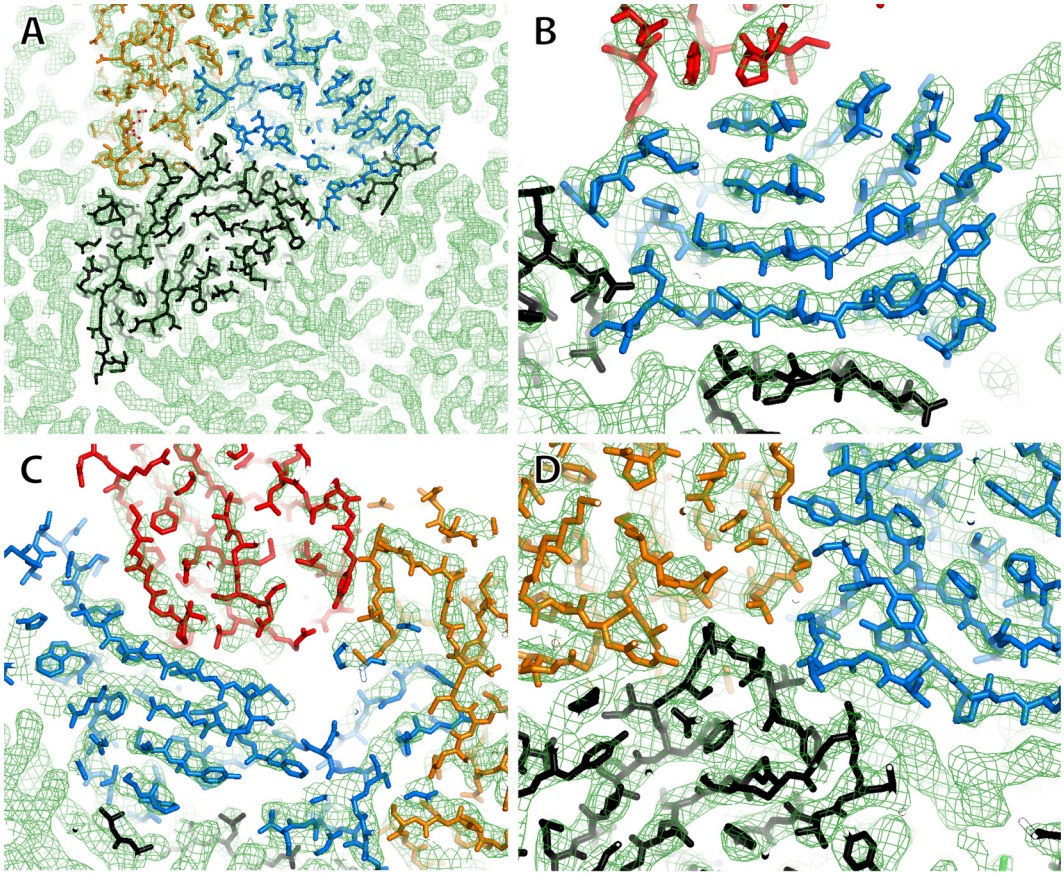

FIG 3 Quality of the electron density map and fit of the refined model for the PVSS21E complex. (A) A slice through the model and the map (near the inner surface of the capsid) shows the icosahedral 5-3-3 triangle (blue, VP1; orange, VP2; black, VP3). (B) The separation of beta strands is clear, and some large side chains have a distinct density. (C) The PVSS21E model (red) binds in a cleft between the C beta strand of VP1 and the EF loop of VP2. (D) The interface between protomers is shown in close-up view.

tion). The latter statistic, calculated as a function of the resolution shell, was used to determine a resolution limit for each refinement.

It should be emphasized that all of the Fourier agreement statistics are primarily intended to monitor convergence, since their exact values unavoidably depend on the choice of masked density that is included in the refinement standard. To ensure that each atomic model agrees acceptably well with idealized stereochemical standards, Fourier amplitudes and phase agreements were weighted versus the Refmac5 stereochemical potentials in a way that achieved root-mean-square (RMS) bond length errors in the range of 0.008 to 0.012 Å and bond angle errors in the range of 1.771 to 2.346°.

TABLE 2 VHH core models

VHH	No. of amino acids[a]	Core PDB accession no.	Main chain (renumbered and mutated) residues[b]
PVSP6A	1–120	4BEL	4–7, 11–24, 34–38, 43–51, 58–96, 110–119
PVSS8A	1–127	4I0C	12–24, 35–39, 46–69, 75–98, 114–118
PVSP19B	1–123	1I3U	2–24, 33–38, 43–51, 54–118
PVSS21E	1–121	3QXU	3–26, 33–38, 45–50, 57–67, 77–93, 113–118
PVSP29F	1–129	1QD0	4–7, 12–22, 34–40, 46–49, 52–53, 58–69, 78–99, 115–127

[a] The number of amino acids in the atomic model, typically including between 1 and 3 ordered histidine residues from the His_6 tag at the carboxyl terminus.
[b] The residue numbers correspond to the sequence of the antipoliovirus VHH.

Contact footprint of the VHHs on the virus surface. In all five VHH complexes, the neutralizing VHHs bind in the canyon, close to the quasi-3-fold axis that is located at the center of the icosahedral triangle having a 5-fold axis and two 3-fold axes at its corners (the 5-3-3 icosahedral triangle) (Fig. 1). The quasi-3-fold axis is the point where VP1 and VP2 from the leftmost biological protomer meet with VP3 from the rightmost protomer. Ink-blot pictures (Fig. 5 and 6) show that all five VHH contact footprints on poliovirus cover similar areas (Fig. 5A to E) nestled into the deep cleft of the canyon, a location that is typically inaccessible to conventional antibodies. This also corresponds to the site of PVR binding (Fig. 5F).

Although the C terminus of the VHH is oriented away from the virus in all cases, nearly every other surface feature on the VHHs was seen to bind in at least one of the complexes (Fig. 5A to E). Since the VHHs are small enough to fit in the reentrant surface of the canyon, they can also use a much larger portion of their surface area in binding. Every VHH does bind with its N terminus (and three sequence-variable loops) in contact with the virus surface. However, except for that constraint,

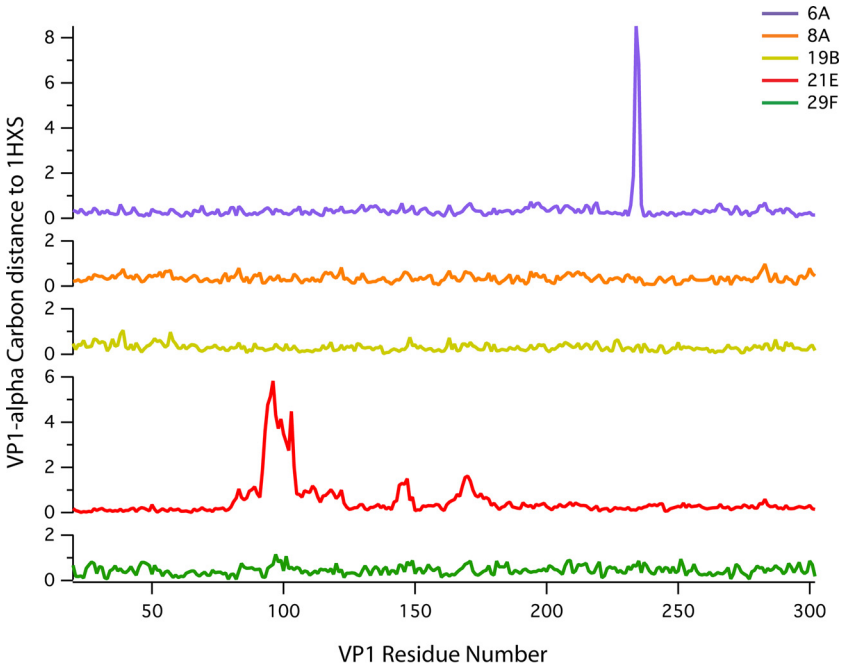

FIG 4 Changes in capsid protein VP1 that result from VHH binding. The alpha-carbon coordinates for VP1 in each of the five VHH-poliovirus complexes are compared with those in the poliovirus crystal structure (PDB accession number 1HXS). Each plot indicates the magnitude of the alpha-carbon difference, expressed as a function of residue number. No meaningful differences occurred in the complexes with PVSS8A, PVSP19B, or PVSP29F. In the PVSP6A complex, a large difference is seen near the doorstop region, around residues 233 to 236. The doorstop is predominantly in a down conformation in the structure with PDB accession number 1HXS but is held in an up conformation in the complex with PVSP6A. For the poliovirus complex with PVSS21E, marked differences in VP1 are seen in the B and C beta strands, the BC, EF, DE, and HI loops, and the CD helix.

there is otherwise no consistency in the orientation of the VHH about its long axis or in the angle that the long axis makes with the virus surface (Fig. 1 and 5). Correspondingly, there is no consistency with which specific polypeptide segments of a VHH molecule are used for binding to each feature on the poliovirus surface (Fig. 6).

Among the detailed contacts between poliovirus and the five neutralizing VHHs (see Table S1 in the supplemental material), there are several structures on the virus surface that consistently participate in binding with all five VHH ligands. Thus, in all five VHH complexes, extensive contacts are seen with a portion of the EF loop of VP2 (around residues 138 to 142), with the GH loop of VP1 (residues 209 to 237), with the EF loop of VP1 (residues 160 to 180), with the C beta strand of VP1 (and vicinity; residues 102 to 115), and with the proximal portion of the C-terminal extension of VP1 (near residue 280) (Fig. 7). Indeed, Leu228 and Val166 (belonging to the GH and EF loops of VP1, respectively) appear on all five lists of interatomic contacts. All five of the above-named polypeptide segments belong to the protomer that occupies the leftmost half of the 5-3-3 icosahedral triangle. Aside from the five common structural elements that are bound by all five VHHs, there are certain other structures on the capsid surface (mostly from the eastern half of the 5-3-3 triangle) that contact a VHH molecule in only one or a few of the five complexes. This is reflected by the variability in VHH position and orientation within the canyon (as shown by Fig. 5). Structural elements that are bound by one or only a few of the VHHs include the BC loop of VP1 (from the leftmost protomer; PVSS21E), the (distal) C-terminal extension of VP1 (from the rightmost protomer; PVSP6A and PVSP29F), the GH loop of VP3 (from the rightmost protomer; PVSS8A, PVSP19B, and PVSP29F), and the knob-like insertion in the VP3 B beta strand (from the rightmost protomer; PVSP6A).

How poliovirus changes when bound to VHHs. To better understand the VHH-based neutralization, we were particularly interested in understanding how the poliovirus structure might change in response to VHH binding. In four of the five VHH complexes (all except that with PVSS21E), the poliovirus structure is nearly indistinguishable from that of the native virus, except for a few specific spots where there are highly localized changes caused by direct binding to the VHHs. This similarity can be seen in a plot of alpha-carbon differences, plotted as a function of residue number (Fig. 4).

The most notable structural difference in the four native-like complexes occurs in the so-called doorstop region of the GH loop of VP1 (residues 233 to 236). In previous poliovirus crystal structures, these doorstop residues have usually been present in a mixture of up and down conformations (as detailed by Strauss et al. [19]), with the predominant conformation being up in some cases (e.g., the structure with PDB accession number 2PLV) and down in other cases (e.g., the structure with PDB accession number 1 HXS). In the picornavirus literature, the conformation of the doorstop is hypothesized to help to control the presence or absence of the pocket factor in the hydrophobic core of VP1 (28). It is easy to see how direct contacts with a VHH (Fig. 7; see also Table S1 in the supplemental material) or the lack of direct contacts could shift the proportions of these two states without creating strain. Thus, the doorstop is predominantly in the down conformation in the PVSP19B, PVSS21E, and PVSP29F complexes and in the up conformation in the PVSP6A complex. PVSS8A was

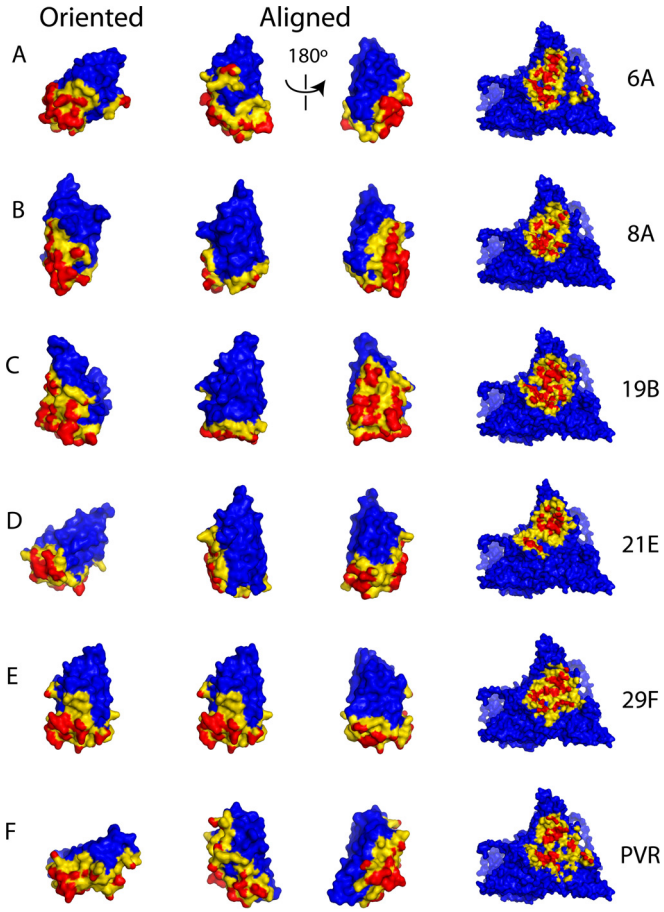

FIG 5 Surface representations show intermolecular contact areas (footprints) between poliovirus and its five neutralizing VHHs. The color coding indicates the distance of the closest approach in each complex (red, 5 Å or closer; yellow, 5 to 9 Å). Domain 1 of poliovirus receptor CD155 (PVR) is included for comparison. In the leftmost column (Oriented), each VHH is shown in its binding orientation relative to the frame of reference of the virus. The rightmost column shows the corresponding footprint of each VHH on the poliovirus surface. Despite the variety of VHH orientations, all five VHHs (and PVR) bind to similar locations in the center of the 5-3-3 icosahedral triangle, deep in the canyon. To facilitate comparisons, the two middle columns (Aligned) show isolated VHH molecules aligned with one another. Clearly, each VHH uses a different set of loops and beta strands to interact with the viral capsid.

modeled as the down conformation, but the density suggests a mixture. These positions are clearly influenced by localized interactions with residues of the VHH (Fig. 7; see also Table S1 in the supplemental material).

Binding to PVSS21E changes the structure of VP1. Although the binding of four out of five of the VHHs leaves the native poliovirus structure substantially unperturbed, VHH PVSS21E, which is the weakest of the neutralizers, alters the structure of VP1 in significant ways. This is evident from the plot of alpha-carbon differences (Fig. 4) relative to the alpha carbons in parental strain Mahoney (PDB accession number 1HXS) and motivated us to omit much of VP1 from the structurally restrained residues during refinement. Unlike the other four VHH complexes, the binding of PVSS21E involves extensive contacts with the BC loop of VP1 (Fig. 7; see also Table S1 in the supplemental material). These contacts change the loop conformation markedly (so that the main chain trace at the top of the BC loop runs perpendicularly to its previous path) and propagate structural differences to the B and C beta strands. Correlated with this movement, we also see alterations in the positions of the EF loop of VP1 (which mediates contacts with the neighboring VP1 beta barrel) with the DE and HI loops of VP1 (which mediate the interprotomer contacts around the 5-fold axis) and in the B beta strand, C beta strand, and CD helix of VP1 (which must reflect small differences in the disposition of beta barrels).

Notably, the regions of VP1 that change in the PVSS21E complex are the same areas of VP1 that were previously seen to move (to a much greater extent) in the picornavirus enterovirus 71 (EV71) upon irreversible expansion of the capsid to form an 80S-like particle and in the irreversible expansion of coxsackievirus A16 (CAV16) and poliovirus to form the 135S particle (28–30). The expansion trajectory is likely to be icosahedrally symmetric and qualitatively similar in all picornaviruses. The observation that PVSS21E binding causes changes in the very same areas leads us to imagine that the PVSS21E-poliovirus complex has sampled and stabilized a point along the expansion trajectory that is clearly distinguishable from that in the unperturbed native structure but not too far away from it (see below).

We should note that the density for the pocket factor in the PVSS21E complex is different in appearance from that in the crystal structures, with the open hydrophilic end of the pocket factor molecule being too disordered to see. Conformational changes in the PVSS21E pocket factor would be plausible, owing to the changes that we see in the shape of the pocket. However, none of our cryo-EM maps have sufficient resolution to show the pocket factor clearly, which makes it impossible to draw reliable conclusions about the pocket factor conformation.

DISCUSSION

In undertaking the structural studies of these five neutralizing VHHs, we endeavored to shed light on the repertoire of binding modes and determine the mechanism of action of neutralizing antipoliovirus VHHs. Here we present some striking observations, discuss their significance, and offer some explanations for their roles in the mechanism of neutralization. Finally, we offer suggestions into the future use of VHHs as standard reagents in vaccine development.

VHHs bind similar sites on poliovirus that overlap the receptor-binding site. When looking at all five VHH-poliovirus complexes, it is immediately clear that all VHHs bind near the quasi-3-fold axis on the virus surface and that all the VHH binding sites overlap extensively with the binding site for the receptor. The similarities in the observed binding site for the neutralizing VHHs may be explained to be the result of the two selection criteria used in screening the phage library and VHHs (during the initial VHH selection). The first criterion was the selection of phages expressing VHHs that bound tightly to immobilized poliovirus. This selection would be expected to favor those VHHs that bound to deep depressions in the virus surface, as this would allow a greater buried surface area and thus a higher affinity. By similar arguments, this selection also accounts for the observation that an unusually large percentage of the surface of the VHHs is involved in interaction with the virus, even though a different portion of the VHH surface is involved in each VHH. However, this observation alone cannot explain the extensive overlap with the receptor-binding site, because there are many areas in the canyon and the saddle-

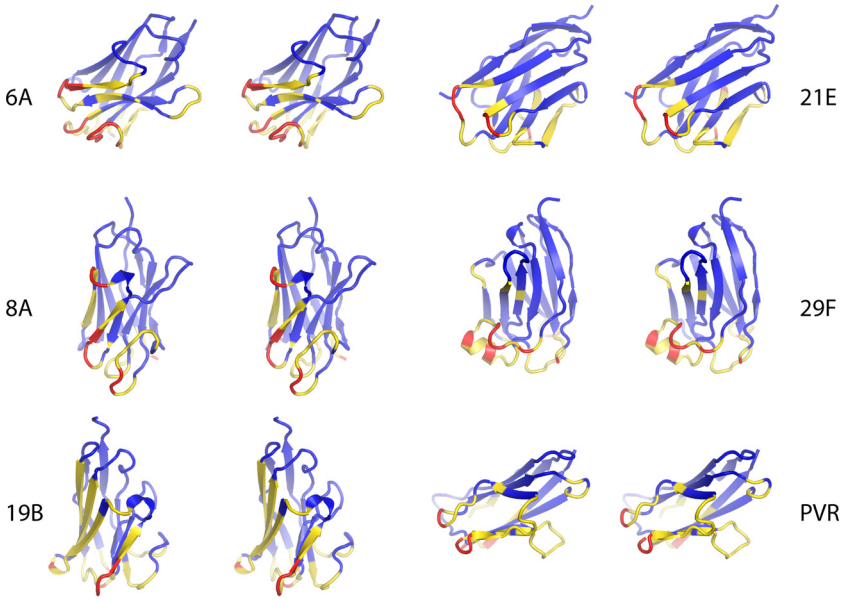

FIG 6 Atomic models for the five neutralizing VHHs are shown in stereo as ribbon representations. Domain 1 of poliovirus receptor CD155 (PVR) is included for comparison. As in Fig. 5 (left column), each model is shown in its binding orientation relative to the frame of reference of the virus and is color coded by its distance of closest approach to the virus surface (red, 5 Å or closer; yellow, 5 to 9 Å).

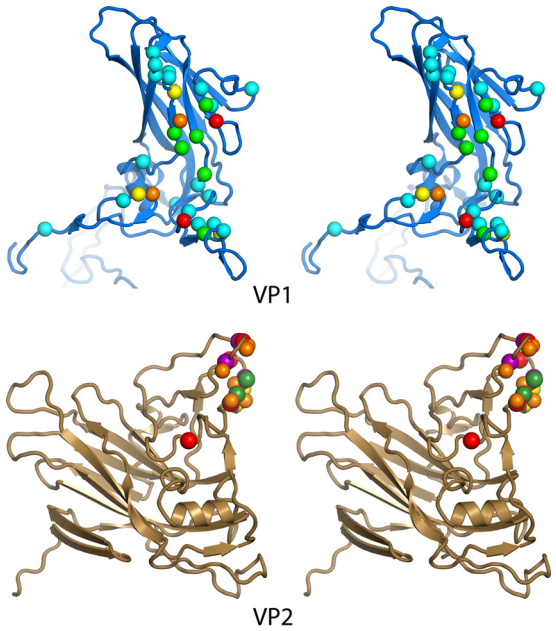

FIG 7 Amino acids in VP1 and VP2 that contact the five neutralizing VHHs directly. In VP1 (blue ribbons, viewed in stereo), the contacting residues are indicated by colored spheres. Common contact areas include the EF and GH loops, the carboxyl-terminal extension, and the vicinity of beta strand C. The sphere color indicates the number of VHH-poliovirus complexes (out of five) in which the corresponding amino acid contacts a VHH directly. Cyan, green, yellow, orange, and red represent one through five contacts, respectively. In VP2 (bronze ribbons, in stereo), contacts with all five VHHs are indicated along a single main chain trace and are color coded by complex. Thus, the spheres on VP2 indicate contact sites with PVSP6A (purple), PVSS8A (orange), PVSP19B (yellow), PVSS21E (red), and PVSP29F (green). Most of these common contact areas in the virus change conformation or become disordered upon expansion of the capsid.

shaped depression across the 2-fold axes where the VHHs could bind with a similarly extensive binding area. We therefore attribute the overlap with the receptor-binding site and the contact with five specific areas (four of which undergo a change upon virus expansion) to the subsequent selection criterion of tightly binding VHHs that are capable of strongly neutralizing the infectivity of the virus. It would be tempting to speculate that selection for the ability to neutralize the virus would select for VHHs that simply block attachment of the receptor sterically. However, several of the VHHs (e.g., PVSP6A and PVSP29F) have been shown to be capable of neutralizing virus infectivity at concentrations well below their K_Ds (equilibrium dissociation constants), suggesting that simple steric exclusion is not the only mechanism by which they inhibit infectivity.

Why VHHs and PVR have similar sites but dissimilar effects. Despite the similarity in the binding footprints of PVR and VHHs (Fig. 1 and 5), the binding of these two classes of ligands has essentially opposite effects. Thus, the binding of the VHHs stabilizes the virus structure against thermally induced expansion and neutralizes infectivity, whereas the binding of the receptor leads to the destabilization of the native structure and expansion to form the 135S particle and promotes infection. The present discussion helps to clarify why that is the case.

(i) Effects of receptor binding. Receptor binding has been shown to cause structural rearrangements that alter the interface between 5-fold-related protomers and result in the loss of the pocket factor, but without causing particle expansion when receptor binding occurs at a low temperature (19). Moreover, when small-molecule antivirals (which bind in the pocket more tightly than the pocket factor does and which highly stabilize the virion against thermally induced expansion) are bound to virus, the presence of the antiviral blocks receptor binding at low temperatures (31). This implies that the virus surface must be changed and that the pocket factor must be released from the pocket, in order to

bind PVR with a high affinity. Based on these observations, we have postulated that the structural changes and the release of the pocket factor, which are associated with receptor binding, leave the complex poised for much larger changes, associated with expansion, when the complex is incubated at physiological temperature (19).

(ii) Effects of binding strongly neutralizing VHHs: neutralization mechanism. In contrast, the binding of the most effective neutralizing VHHs (which are stabilizing) perturbs the virus as little as possible and the pocket remains occupied. The common contacts shared by all five VHHs (the EF loops of VP2, the EF and GH loops of VP1, and the C beta strand and C-terminal extension of VP1) include important stabilizers of the native structure that stabilize by binding to neighboring beta barrels. The importance of these contact areas for neutralization is further supported by the observation that all of the identified escape mutations on the surface of the VHH-resistant escape mutant viruses were located within the same five structural elements (6). Thus, the escape mutation sites that were exposed included residues 102, 109, 150, 166, 168, 222, 223, and 228 of VP1 and residues 139 and 142 of VP2 but included no exposed residues outside the five-element common footprint. (All additional escape mutation sites that were buried in the interior of the capsid involved interfaces that change during virus expansion.) We therefore propose that the VHHs prevent the movement of those controlling elements by adding additional stabilizing contacts to them. One effect of immobilizing those polypeptides in place could be to prevent the shifting of capsid protein beta barrels that otherwise occurs during expansion, once the stabilizing contacts have been removed. Alternatively, the immobilization of the peptide segments may act by preventing the release of the pocket factor. Thus, all five structural elements that the neutralizing VHHs bind in common (possibly except for the distal GH loop of VP1) lie in direct contact either with the pocket factor itself or with hydrophobic residues that line the pocket. Computational dynamics simulations by Li et al. (32) on a complex between rhinovirus 14 and the capsid-binding drug WIN52084 showed that the pocket occupant can snake its way out of the pore (the outer, hydrophilic open end of the pocket) without significantly perturbing the native virus structure, except in three specific, localized areas of VP1. These areas included the C beta strand and the EF loop (both of which are common VHH contact areas) and the middle of the G beta strand. The two proposed mechanisms are obviously not exclusive, and both could explain the ability of the VHHs to neutralize at a low copy number. The stabilization provided by binding to a small number of VHHs, along with the constraints of the tightly packed icosahedral surface, could be sufficient to prevent the expansion that otherwise would be induced by a receptor molecule bound at another site. This is entirely consistent with previous observations that all the poliovirus structures that we have observed to date, with the exception of structures associated with RNA release, preserve icosahedral symmetry.

The curious case of PVSS21E. Curiously, in the case of PVSS21E, which is by far the worst neutralizer in the group, the structural changes in the virus are more significant. Thus, significant changes are seen in the top surface of VP1, involving the B and C beta strands, the BC and DE loops, and the CD helix, though most of the remainder of the VP1 beta barrel remains substantially unchanged. Fortunately, this structure is the highest-resolution structure in the group (3.8 Å), and we are therefore able to model its changes confidently. It is worth noting that the changes due to PVSS21E binding could be accommodated by changes in the pocket factor conformation and that the pocket factor remains bound. These are less extreme than the structural changes that are caused by receptor binding, which totally occlude the pocket, expelling the pocket factor and preventing its rebinding. Moreover, like the other four VHHs, PVSS21E binds to five key regions of the virus surface, four of which change during expansion. This leads to the suggestion that despite causing serious perturbations, PVSS21E might neutralize the virus by a mechanism that is similar to that of the other four VHHs.

The PVSS21E-poliovirus complex as a window to early stages of the process of particle expansion. One can think of the PVSS21E-virus complex as a very early reversible stage in the expansion process. As such, there is a balance between the stabilizing effect of PVSS21E (thereby blocking infection) and destabilization of the virus associated with the structural changes required for expansion. PVSS21E binding provides stabilizing contacts within regions that change during expansion and prevents the pocket factor from being released. This view reinforces the notion (which was originally proposed from the observation that the virus breathes and which is discussed in more detail by Strauss et al. [19]) that expansion is a multistep process and that structural studies of the virus (particularly in complex with different ligands) sometimes allow us to sample the conformational repertoire of the virus by trapping different stages along the multistep pathway.

Neutralizing VHHs as standard quality control reagents for vaccine manufacture. Traditionally, panels of antibodies have been used to measure the D-antigen content as a measure of the potency of vaccine lots during inactivated polio vaccine (IPV) production (33, 34). Although they have proven to be very useful, the current panels of antibodies are imperfect, in that different manufacturers use different proprietary panels that are specific to the strains used by the manufacturer and different assay formats, leading to difficulties in comparing the actual D-antigen contents of vaccine lots from different manufacturers. Moreover, the current panels are poorly reactive with formalin-inactivated preparations using Sabin strains, which are expected to replace wild-type strains as seed stocks for new manufactures. As the number of manufacturers of IPV increases and production facilities become distributed worldwide, there is an increasing need for standard reagents, which has recently been formalized in recommendations from WHO and the Bill and Melinda Gates Foundation advisory group PATH (35, 36). We would argue that the VHHs deserve serious consideration as replacements for the currently used panels of antibodies. Thus, they can be stored as cDNA (and therefore are less susceptible to loss), they are cheaper to produce in bulk, they are presently less constrained by intellectual property concerns, and, because they bind to a highly conserved site that is a site of significant conformational change during the D-to-C conversion, they are less likely to be strain specific and more likely to serve as a better determinant of the D-antigen content of vaccine lots.

ACKNOWLEDGMENT

We declare no conflict of interest.

FUNDING INFORMATION

HHS | National Institutes of Health (NIH) provided funding to James M. Hogle under grant number AI020566. Fonds Wetenschappelijk Onderzoek (FWO) provided funding to Lise Schotte. Alexander von Humboldt-Stiftung (Humboldt Foundation) provided funding to Mike Strauss.

REFERENCES

1. **Hamers-Casterman C, Atarhouch T, Muyldermans S, Robinson G, Hamers C, Songa EB, Bendahman N, Hamers R.** 1993. Naturally occurring antibodies devoid of light chains. Nature **363:**446–448. http://dx.doi.org/10.1038/363446a0.
2. **Arbabi Ghahroudi M, Desmyter A, Wyns L, Hamers R, Muyldermans S.** 1997. Selection and identification of single domain antibody fragments from camel heavy-chain antibodies. FEBS Lett **414:**521–526. http://dx.doi.org/10.1016/S0014-5793(97)01062-4.
3. **Conrath KE, Lauwereys M, Galleni M, Matagne A, Frere JM, Kinne J, Wyns L, Muyldermans S.** 2001. Beta-lactamase inhibitors derived from single-domain antibody fragments elicited in the Camelidae. Antimicrob Agents Chemother **45:**2807–2812. http://dx.doi.org/10.1128/AAC.45.10.2807-2812.2001.
4. **Thys B, Schotte L, Muyldermans S, Wernery U, Hassanzadeh-Ghassabeh G, Rombaut B.** 2010. In vitro antiviral activity of single domain antibody fragments against poliovirus. Antiviral Res **87:**257–264. http://dx.doi.org/10.1016/j.antiviral.2010.05.012.
5. **Schotte L, Strauss M, Thys B, Halewyck H, Filman DJ, Bostina M, Hogle JM, Rombaut B.** 2014. Mechanism of action and capsid-stabilizing properties of VHHs with an in vitro antipolioviral activity. J Virol **88:**4403–4413. http://dx.doi.org/10.1128/JVI.03402-13.
6. **Schotte L, Thys B, Strauss M, Filman DJ, Rombaut B, Hogle JM.** 2015. Characterization of poliovirus neutralization escape mutants of single-domain antibody fragments (VHHs). Antimicrob Agents Chemother **59:**4695–4706. http://dx.doi.org/10.1128/AAC.00878-15.
7. **Chow M, Newman JF, Filman D, Hogle JM, Rowlands DJ, Brown F.** 1987. Myristylation of picornavirus capsid protein VP4 and its structural significance. Nature **327:**482–486. http://dx.doi.org/10.1038/327482a0.
8. **Tsang SK, McDermott BM, Racaniello VR, Hogle JM.** 2001. Kinetic analysis of the effect of poliovirus receptor on viral uncoating: the receptor as a catalyst. J Virol **75:**4984–4989. http://dx.doi.org/10.1128/JVI.75.11.4984-4989.2001.
9. **De Sena J, Mandel B.** 1977. Studies on the in vitro uncoating of poliovirus. II. Characteristics of the membrane-modified particle. Virology **78:**554–566.
10. **Fricks CE, Hogle JM.** 1990. Cell-induced conformational change in poliovirus: externalization of the amino terminus of VP1 is responsible for liposome binding. J Virol **64:**1934–1945.
11. **Fenwick ML, Cooper PD.** 1962. Early interactions between poliovirus and ERK cells: some observations on the nature and significance of the rejected particles. Virology **18:**212–223. http://dx.doi.org/10.1016/0042-6822(62)90007-7.
12. **Danthi P, Tosteson M, Li QH, Chow M.** 2003. Genome delivery and ion channel properties are altered in VP4 mutants of poliovirus. J Virol **77:**5266–5274. http://dx.doi.org/10.1128/JVI.77.9.5266-5274.2003.
13. **Brandenburg B, Lee LY, Lakadamyali M, Rust MJ, Zhuang X, Hogle JM.** 2007. Imaging poliovirus entry in live cells. PLoS Biol **5:**e183. http://dx.doi.org/10.1371/journal.pbio.0050183.
14. **Hummeler K, Hamparian VV.** 1958. Studies on the complement fixing antigens of poliomyelitis. I. Demonstration of type and group specific antigens in native and heated viral preparations. J Immunol **81:**499–505.
15. **Beale AJ, Mason PJ.** 1962. The measurement of the D-antigen in poliovirus preparations. J Hyg (Lond) **60:**113–121. http://dx.doi.org/10.1017/S002217240003936X.
16. **Belnap DM, McDermott BM, Jr, Filman DJ, Cheng N, Trus BL, Zuccola HJ, Racaniello VR, Hogle JM, Steven AC.** 2000. Three-dimensional structure of poliovirus receptor bound to poliovirus. Proc Natl Acad Sci U S A **97:**73–78. http://dx.doi.org/10.1073/pnas.97.1.73.
17. **He Y, Mueller S, Chipman PR, Bator CM, Peng X, Bowman VD, Mukhopadhyay S, Wimmer E, Kuhn RJ, Rossmann MG.** 2003. Complexes of poliovirus serotypes with their common cellular receptor, CD155. J Virol **77:**4827–4835. http://dx.doi.org/10.1128/JVI.77.8.4827-4835.2003.
18. **Filman DJ, Syed R, Chow M, Macadam AJ, Minor PD, Hogle JM.** 1989. Structural factors that control conformational transitions and serotype specificity in type 3 poliovirus. EMBO J **8:**1567–1579.
19. **Strauss M, Filman DJ, Belnap DM, Cheng N, Noel RT, Hogle JM.** 2015. Nectin-like interactions between poliovirus and its receptor trigger conformational changes associated with cell entry. J Virol **89:**4143–4157. http://dx.doi.org/10.1128/JVI.03101-14.
20. **Li X, Mooney P, Zheng S, Booth CR, Braunfeld MB, Gubbens S, Agard DA, Cheng Y.** 2013. Electron counting and beam-induced motion correction enable near-atomic-resolution single-particle cryo-EM. Nat Methods **10:**584–590. http://dx.doi.org/10.1038/nmeth.2472.
21. **Mindell JA, Grigorieff N.** 2003. Accurate determination of local defocus and specimen tilt in electron microscopy. J Struct Biol **142:**334–347. http://dx.doi.org/10.1016/S1047-8477(03)00069-8.
22. **Tang G, Peng L, Baldwin PR, Mann DS, Jiang W, Rees I, Ludtke SJ.** 2007. EMAN2: an extensible image processing suite for electron microscopy. J Struct Biol **157:**38–46. http://dx.doi.org/10.1016/j.jsb.2006.05.009.
23. **Scheres SH.** 2012. RELION: implementation of a Bayesian approach to cryo-EM structure determination. J Struct Biol **180:**519–530. http://dx.doi.org/10.1016/j.jsb.2012.09.006.
24. **Li X, Grigorieff N, Cheng Y.** 2010. GPU-enabled FREALIGN: accelerating single particle 3D reconstruction and refinement in Fourier space on graphics processors. J Struct Biol **172:**407–412. http://dx.doi.org/10.1016/j.jsb.2010.06.010.
25. **Scheres SH, Chen S.** 2012. Prevention of overfitting in cryo-EM structure determination. Nat Methods **9:**853–854. http://dx.doi.org/10.1038/nmeth.2115.
26. **Grigorieff N.** 2007. FREALIGN: high-resolution refinement of single particle structures. J Struct Biol **157:**117–125. http://dx.doi.org/10.1016/j.jsb.2006.05.004.
27. **Murshudov GN, Vagin AA, Dodson EJ.** 1997. Refinement of macromolecular structures by the maximum-likelihood method. Acta Crystallogr D Biol Crystallogr **53:**240–255. http://dx.doi.org/10.1107/S0907444996012255.
28. **Wang X, Peng W, Ren J, Hu Z, Xu J, Lou Z, Li X, Yin W, Shen X, Porta C, Walter TS, Evans G, Axford D, Owen R, Rowlands DJ, Wang J, Stuart DI, Fry EE, Rao Z.** 2012. A sensor-adaptor mechanism for enterovirus uncoating from structures of EV71. Nat Struct Mol Biol **19:**424–429. http://dx.doi.org/10.1038/nsmb.2255.
29. **Ren J, Wang X, Hu Z, Gao Q, Sun Y, Li X, Porta C, Walter TS, Gilbert RJ, Zhao Y, Axford D, Williams M, McAuley K, Rowlands DJ, Yin W, Wang J, Stuart DI, Rao Z, Fry EE.** 2013. Picornavirus uncoating intermediate captured in atomic detail. Nat Commun **4:**1929. http://dx.doi.org/10.1038/ncomms2889.
30. **Butan C, Filman DJ, Hogle JM.** 2014. Cryo-electron microscopy reconstruction shows poliovirus 135S particles poised for membrane interaction and RNA release. J Virol **88:**1758–1770. http://dx.doi.org/10.1128/JVI.01949-13.
31. **Dove AW, Racaniello VR.** 2000. An antiviral compound that blocks structural transitions of poliovirus prevents receptor binding at low temperatures. J Virol **74:**3929–3931. http://dx.doi.org/10.1128/JVI.74.8.3929-3931.2000.
32. **Li Y, Zhou Z, Post CB.** 2005. Dissociation of an antiviral compound from the internal pocket of human rhinovirus 14 capsid. Proc Natl Acad Sci U S A **102:**7529–7534. http://dx.doi.org/10.1073/pnas.0408749102.
33. **Salk J, Cohen H, Fillastre C, Stoeckel P, Rey JL, Schlumberger M, Nicolas A, van Steenis G, van Wezel AL, Triau R, Saliou P, Barry LF, Moreau JP, Merieux C.** 1978. Killed poliovirus antigen titration in humans. Dev Biol Stand **41:**119–132.
34. **World Health Organization.** 2002. Recommendations for the production and control of poliomyelitis vaccine (inactivated). WHO technical report series, no. 910. World Health Organization, Geneva, Switzerland. http://www.who.int/biologicals/publications/trs/areas/vaccines/polio/WHO_TRS_910_Annex2_polioinactivated.pdf.
35. **World Health Organization.** 2014. Recommendations to assure the quality, safety and efficacy of poliomyelitis vaccine (inactivated). World Health Organization, Geneva, Switzerland. http://www.who.int/biologicals/IPV_FINAL_for_BS2233_07072014(2).pdf.
36. **PATH.** 2015. Vaccines for the future. PATH, Seattle, WA.